www.czasopisma.pan.pl PAN www.journals.pan.pl

Opto-Electronics Review 25 (2017) 326–336

Contents lists available at ScienceDirect

Opto-Electronics Review

journal homepage: http://www.journals.elsevier.com/opto-electronics review

Robust geometric, phase and colour structured light projection system calibration

K. Szelag[a,*], G. Maczkowski[a], R. Gierwialo[a], A. Gebarska[b], R. Sitnik[a]

[a] Faculty of Mechatronics Warsaw University of Technology, Warsaw, Poland
[b] SMARTTECH Poland Warsaw, Poland

ARTICLE INFO

Article history:
Received 14 September 2016
Accepted 9 January 2017
Available online 9 November 2017

Keywords:
Structured light
Colour calibration
Geometric calibration
Low cost scanner
Simple calibration

ABSTRACT

This paper introduces a new comprehensive procedure for both geometric and colour calibration of structured light system. In order to perform both geometric and colour calibration procedure, a new calibration artifact is proposed. The intrinsic and extrinsic parameters of projector and camera are estimated by using an extended pinhole camera model with a tangential and radial distortion. Camera image plane coordinates are obtained by extracting features from images of a calibration artifact. Projector image plane coordinates are calculated on the basis of continuous phase maps obtained from a fringe pattern phase reconstruction procedure. In order to stereo calibrate camera-projector system, pairs of corresponding image plane points are calculated with subpixel accuracy. In addition, one of three pattern views is used in colour calibration. RGB values of a colour field pattern detected by camera and their reference values are compared. This comparison leads to derivation of a colour transformation matrix. The performance of the proposed method is tested by measuring plane, sphere and distance reference. Also 360 degrees complex object 3D model from a set of measurements is obtained. Residual mean errors for all tests performed are calculated.

1. Introduction

Non-contact 3D measurement is one of the most rapidly expanding field of modern vision techniques with many applications in robotics [1], medicine [2], manufacturing [3] and inspection [4]. Among many techniques used in these applications, structured light based (SLS) are especially popular [5]. During SLS measurement procedure, the specified pattern of light is projected on the object surface. Stereo systems in that case differ from classic camera-camera applications by presence of a DLP projector in substitute of a second camera. With known structure of a light pattern, each pixel of projecting-plane could be easily found on the camera image. As a result of this modification, fundamental point correspondence problem in a stereo camera system could be easily resolved. Various pattern structures and pixel coding methods presented and classified in Ref. [6] could be used to achieve this goal. As a result of the measurement, large set of points (equal to detector resolution) with corresponding 3D coordinates is obtained. In well calibrated systems micrometer accuracy could be achieved [7]. Fast data acquisition, non-contact character and high accuracy make structured light methods well suited with many modern applications. However, one of main disadvantages of structured light systems is a weak colour representation of an object texture due to additional light source (DLP projector) in the measurement system. Nowadays, many methods of proper colour calibration and white balance correction in SLS system are developed. Among them many uses known spectral reflectance characteristics of a colour pattern illuminated by a standardized light source (D65) [8]. Therefore, there are no procedures which allow to calibrate system geometrically with object texture colour correction using same calibration artifact and image sequences.

2. Related work

2.1. Depth reconstruction with projected fringes

Usage of a projector in stereo pair involves proper pixel coordinates coding. Many various techniques could be used in order to perform this action. As an example, bundle adjustment, neural networks, absolute phase or stochastic pattern projection methods may be used [9]. Among many approaches, the absolute phase coding can provide high accuracy combined with easy implementation and fast field measurement [10]. Therefore, in the presented research projector pixel addressing with an absolute phase coding is considered. In the most common realization, absolute phase

* Corresponding author.
E-mail addresses: k.szelag@mchtr.pw.edu.pl (K. Szelag), g.maczkowski@mchtr.pw.edu.pl (G. Maczkowski), r.gierwialo@mchtr.pw.edu.pl (R. Gierwialo), ag@smarttech.pl (A. Gebarska), r.sitnik@mchtr.pw.edu.pl (R. Sitnik).

https://doi.org/10.1016/j.opelre.2017.10.001
1230-3402/

code is obtained in two main steps [11]. First step involves projecting a sine-modulated pattern shifted with three of five phase steps [12] and set of Gray codes. On the basis of intensity distribution observed by camera, a continuous phase map is obtained. [13]. During the second step calculated phase value is transformed into projector pixel coordinates (analytic camera-projector model) [14,9] or depth map (experimental model) [11,2] in order to receive real 3D coordinates of the measured object. Data acquisition for experimental approach requires many samples in measurement volume because of a strong correlation between quality of sampling density and measurement accuracy [11]. On the other hand, usage of a projector pinhole model may cause errors due to simplification of the projector mathematical model.

2.2. Camera pinhole model

Camera pinhole model is considered as the state of art in the modern mathematical description of camera. Being a crude and not ideal representation of real object, this model can easily represent perspective transformation in a set of linear or quasi-linear equations [15]. In the presented paper, camera pinhole model is used, with focal length described by the parameters fy and fx, the principal point coordinates Cx and Cy and the scale factor s. In camera pose modeling, rotation and translation are described by the extrinsic matrix E [Eq. (1)]

$$E = \begin{bmatrix} r_{11} & r_{12} & r_{13} & t_1 \\ r_{21} & r_{22} & r_{23} & t_2 \\ r_{31} & r_{32} & r_{33} & t_3 \end{bmatrix}. \quad (1)$$

In the designed system, radial and tangential distortion are considered. Final distortion displacement is calculated as a sum of both distortion factors. Beside the presented model, many approaches of distortion correction may be found in literature. As an example hybrid models [16] and scene based techniques [17] could be mentioned.

2.3. Projector pinhole model

Camera pinhole model described in Section 2.2 could be easily adapted for a DLP projector. Projection, instead of capturing results only in reverse ray directions, which is irrelevant for the pinhole model. Addresses of projector pixels are obtained via absolute phase coding described in Section 2.1. Method presented in this paper uses the projector pinhole model in order to reconstruct real 3D coordinates of a measured object.

2.4. Stereo pair

In stereo system described in this work, the measured object is visible by both the camera and the projector. Stereo calibration with pinhole model of both devices could be performed. Object point global 3D coordinates are transformed by Eq. (1) of each device depending on their position [18]. Therefore, two local coordinate spaces, often called 'device coordinates systems' should be introduced. Mutual location of both devices, marked by transformation Ψ, defines the system arrangement and remains constant during performed measurements. Transformation Ψ describes translation and rotation between devices coordinate systems and could be represented by a 3×4 matrix used to define extrinsic pinhole parameters (Section 2.2). With Ψ known, global device coordinate system could be defined and local-to-global transformation matrices $\Psi 1$, $\Psi 2$ could be calculated. With known intrinsic device parameters and relative positions, 3D shape reconstruction may be performed. It is worth mentioning that 3D coordinates obtained during reconstruction are actually located in the global device coordinate system.

2.5. Camera-projector stereo calibration

In order to obtain parameters used in the pinhole model, a proper calibration should be conducted. In the proposed system Zhang's method [19] is used for intrinsic and extrinsic camera calibration. The flat circle grid pattern is imaged by the camera in two specified poses (Fig. 2). For each position of the planar calibration artifact fringe pattern is projected so that continuous phase map could be calculated. Therefore, the projector image coordinates are available for each of the camera image point detected. With a set of corresponding points provided, global Levenberg-Marquardt algorithm [20] is used in order to calculate both intrinsic, extrinsic and mutual parameters.

2.6. Colour reproduction

In the presented research we consider the use of a trichromatic camera equipped with a Bayer filter matrix on top of the imaging sensor [21]. In the most common configuration, the camera registers intensity in three independent spectral channels around red, green and blue regions of the visible spectrum. A colour model predicts camera intensity response for a signal with specific spectral power distribution, given an assumed illumination. Several methods which estimate the camera response curve were developed. Typically they are based on a set of images [22] but using a single image is also reported [23]. Some other interesting solutions include a low-parameter empirical model of a camera response function based on a theoretical analysis and a database of real-world camera responses [24]. The aim of the presented work is to improve the camera colour reproduction. In a real-world working conditions the illumination SPD is not known, so finding the camera spectral response will not be sufficient to predict the colour output. Instead an empirical calibration can be performed which allows to find a relation between the raw camera output and independent colour representation. The most often choice in this regard is a colourimetric model based on the CIE standard [25]. The model was initially used for colour characterization of a flat-bed scanner, but can be also adopted for a camera [26]. The main assumption is that the camera response is linear (or linearized in advance with a lookup table), so that the raw colour signal read from the sensor matrix is proportional to the CIE XYZ coordinates, as in Eq. (2).

$$\begin{bmatrix} X \\ Y \\ Z \end{bmatrix} = Mx \begin{bmatrix} r \\ g \\ b \end{bmatrix} \quad (2)$$

Given the model matrix M it is possible to estimate the camera colour response in the CIE XYZ independent colour space. Consequently, the colour information can be reconstructed in one of many device dependent RGB colour spaces which are most often defined as a linear transformation of the CIE XYZ space, sometimes with an additional gamma correction.

2.7. Nowadays methods and implementations of camera-projector stereo system calibrations.

In Structured-light systems, camera and projector calibration has an important role in high accuracy of final measurements. Aim of this step is to find a relation between pixel 2D image and line in a 3D space. It is a well-known problem. Technique proposed in Ref. [27] uses uncalibrated camera to calibrate projector in order to avoid errors propagation. Other method is using markerless surface but assumes partial kwowledge of camera parameters [28]. In

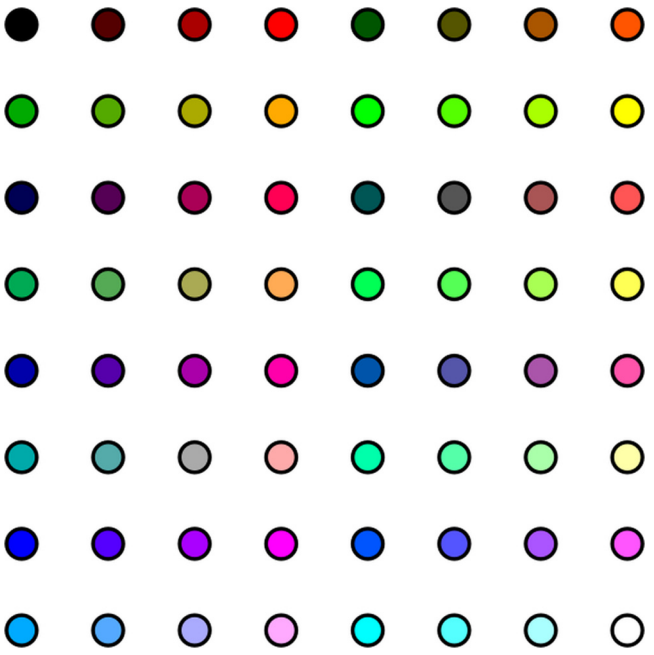

Fig. 1. Layout of the calibration artifact.

Ref. [29] a system with two Kinects provides a complete 3D data of an object. Different approach is proposed in Ref. [30] where the projector is treated as the inverse of a camera with virtual target planes. Otherwise calibration can be performed by illuminating light stripes on the object [31]. In Ref. [32] synthetic fringe patterns in two orthogonal directions are used to calibrate the system. None of the invented methods allow to calibrate system's geometry and colour reproduction using the same calibration artifact.

3. Proposed method

3.1. Proposed planar artifact

In the developed solution, it was important to provide a single pattern for both geometric and colour calibration procedure. The aim was to simplify the calibration process as much as possible and make it available for an unqualified user. Therefore, the custom target pattern was designed in a way that 64 circular markers, spaced equally every 35 mm in both directions are filled with different hues (Fig. 1). The fill colours were chosen so that they cover as much of the camera input colour space as possible. Although, their spread is limited by the capabilities of a printer used to manufacture the target. In the real world experiment, a high-fidelity ink-jet printer was used. However, many solutions use a checkerboard pattern for geometric camera calibration, utilization of circular markers is considered advantageous. Center of a circle in an image can be effectively found with a sub-pixel precision with the use of a gradient based algorithm. Edge detection algorithms used with the checkerboard patterns can cause ambiguities in transition from black and white and vice-versa which reduces the corners position accuracy.

3.2. Data acquisition

Simplicity and short time of data acquisition were considered as main principles. To get both calibration and measurement data we propose the following system setup (Fig. 2).

Medium resolution (≈2MP ix) colour camera and a DLP projector are placed at a distance between 0.4 and 0.6 m from each other. Devices are oriented so their optical axes intersect in the middle of the measurement volume. Angle between the axes α should be in

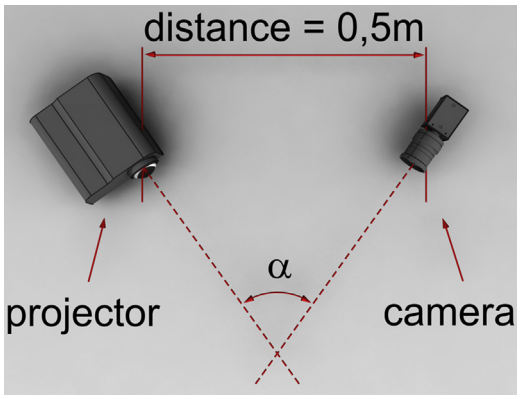

Fig. 2. Geometric setup for camera and projector system, with relative distance, angle and measurement distance. Quantitative values discussion is presented in Section 3.2.

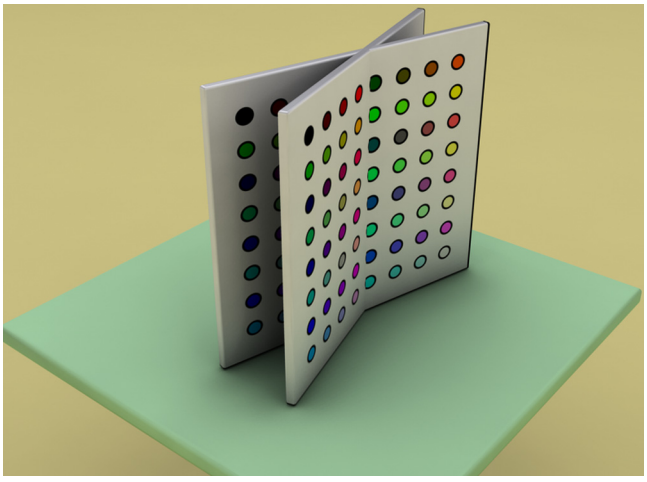

Fig. 3. Calibration artifact positions.

the range from 30º to 45º. [5] With higher angle the measurement accuracy increases but the common field of view of the camera and projector decreases. Proposed angle was chosen empirically based on the performed tests. Obviously both angle and distance should be fixed and constant during the calibration but easy to change when needed. During the system calibration, the calibration artifact locations are shown in Fig. 3. Center of the artifact in each position should be located as close as possible to the intersection of the devices optical axes of the devices. When each marker center is considered as a 3D point (in the global coordinate system), bounding box containing all points could be made. Such bounding box is treated as a measurement volume during following measurements.

3.3. Pairs of corresponding points

To find the transformation between the camera and the projector coordinates, positions of the coresponding points must be determined. In the stereo pair setup the characteristic points are found as the centers of circular markers imaged by both cameras. However, with one camera replaced by the projector, the possibility to determine second view of the calibration artifact is lost and the characteristic points have to be determined in a different way.

3.4. Recovery of projector pixel coordinates

In this work we calculate intrinsic parameters of a camera on two tilted positions of the artifact with respect to the camera's

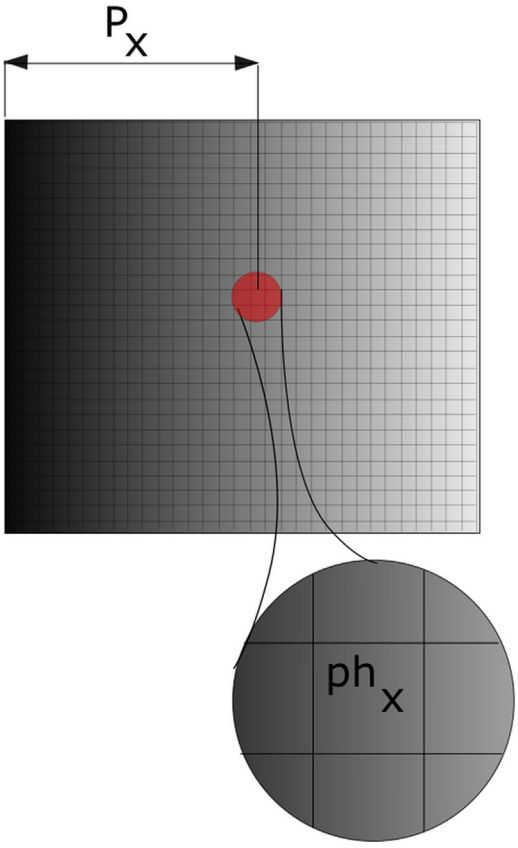

Fig. 4. Continuous phase map with marked projector pixel P_x coordinate.

optical axis. For each view the projector displays a sequence of time-shifted horizontal and vertical sine fringes with corresponding binary gray code values. After recovering and unwrapping phase from the fringe images we can determine the projector pixel coordinates according to the relationships:

$$P_x = \frac{n_{fr} \cdot ph_x}{2\pi} \tag{3}$$

$$P_y = \frac{n_{fr} \cdot ph_y}{2\pi}, \tag{4}$$

where n_{fr} is the sine fringe period, ph_x and ph_y are the phase value in vertical and horizontal direction, respectively (Fig. 4).

When we project fringes on the calibration artifact, the phase on each marker is disturbed by its hue ie. pixel intensity is lower on the marker than on the white background and local contrast decreases. To avoid that influence, we assume that the local nonlinearity of phase distribution is relatively small. On the basis of that assumption we approximate nonlinear distribution of phase in two directions by a linear one. It allows us to calculate phase in the center of each marker using linear interpolation. During that interpolation, we use phase information in midpoint sections between the centre of the marker and its neighbours centers (Fig. 5). In most cases, the resolution of projector's sensor is smaller than camera's sensor so data from projector is re-scaled.

3.5. Coordinate system and 3D reconstruction

Having the calibration performed, both intrinsic extrinsic parameters of devices are known. After recovering projector pixel coordinates coded in continuous phase maps it is possible to achieve projector and camera image plane coordinates for each

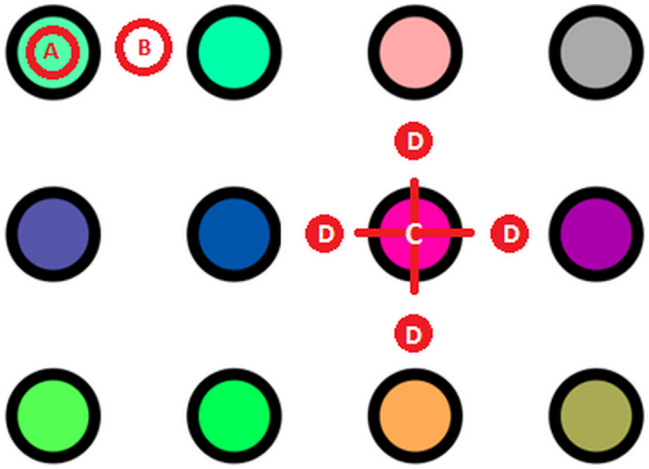

Fig. 5. (A) marker area where phase will be disturbed; (B) area of calibration pattern with accurate phase values; (D) – points which values will be considered in interpolation phase of (C) point.

observed camera pixel. We propose a four step algorithm to reconstruct 3D coordinates of all measured points.

3.5.1. Distortion correction for both camera and projector pixel coordinates

Distortion model, presented in Ref. [33] is used in order to calculate corrected pixel coordinates. A set of n-th order polynomial equations is solved for positive real solutions representing the desired point coordinates.

3.5.2. Pixel's line calculation

For each pixel, the line connecting the device focus point in the device coordinate space and the point projection could be constructed. Line equation could be easily derived from projection equation, as follows:

$$\begin{cases} x = \dfrac{u - P_x}{f_x} \cdot s \\ y = \dfrac{v - P_y}{f_y} \cdot s. \\ z = s \end{cases} \tag{5}$$

For camera and projector, parallel vectors (vc0,vp0) could be calculated.

$$v_{c0,p0} = \left[\frac{u - P_x}{f_x}, \frac{v - P_y}{f_y}, 1 \right]. \tag{6}$$

After normalization, unit vector could be calculated and centre of the device coordinates system [O(0, 0, 0)] could be considered as a point that is on the line (p_{c0}, p_{p0}).

3.5.3. Common coordinates system transformation

Device coordinate system of the camera is chosen as the global coordinate system for measurements. As a result, the local-to-global transformation matrices Ψ1, Ψ2 are defined as:

$$\begin{matrix} \Psi_1 = [I|0] \\ \Psi_2 = \Psi \end{matrix}. \tag{7}$$

Therefore, pixel line vector for the camera vc = vc0, and and pixel line point pc = pc0 remain unchanged. On the other hand, the projector vector and point should be transformed with Ψ matrix

$$\Psi = [R_\Psi | T_\Psi]$$
$$v_p = R_\Psi v_{p0} \quad (8)$$
$$p_p = p_{p0} + T_\Psi$$

3.5.4. Point coordinates reconstruction

With known line equations for each camera-projector pixels pairs, 3D coordinates of measured point could be calculated with the usage of triangulation techniques [34]. Because of noisy data and calibration errors the lines may be skew. Thus, instead of calculating the intersection, the shortest section connecting two lines is calculated, and its midpoint is considered as a result [35].

Defining the camera device coordinate system as the global one does not affect shape reconstruction. We considered that approach to be intuitive and proper.

3.6. Colour calibration

The colour calibration procedure aims to find a model matrix M, as defined in Eq. (2). It can be done empirically by imaging a set of uniform colour patches prepared in a way that their CIE XYZ coordinates are known and can be used as a reference. If CXYZ is a [n × 3] vector of CIE XYZ reference values and Crgb is a vector of camera colour responses for these patches, then Eq. (2) can be rewritten as Eq. (9).

$$M = C^{XYZ} \times (C^{rgb})^{+} \quad (9)$$

In order to find the model matrix, the raw response matrix Crgb must be inverted with the pseudo-inverse approach. The model matrix found this way can be used to estimate the CIE XYZ response for any colour input, assuming that the illumination conditions remain the same. In the presented setup the DLP projector which is used for displaying fringes is also utilized as a light source for colour acquisition. An additional background frame is captured with the projector turned off in order to minimize the influence of variable ambient lighting conditions. This way relatively constant illumination conditions are satisfied. An important issue is the choice of the reference set of colour patches because they should either span the whole colour space of the camera or resemble closely the set of reproduced colours. Application of the pseudo-inverse method means that extrapolation of colours beyond the reference ones can cause big reproduction errors. In many solutions the X-Rite ColourChecker target is used as a reference set of patches because their hues are well defined and stable. However, the developed solution was constrained to use a single calibration artifact for both geometry and colour in order to simplify the calibration process as much as possible (Section 3.1). In order to use the artifact for colour calibration, each colour patch filling the circular marker has to be characterized with the CIE XYZ coordinates. It was achieved by performing a master calibration with the ColorChecker target as a reference. The procedure is the same as described in Section II-F only the CIE XYZ coordinates of the ColourChecker target are known and the values for each marker fill are estimated. The reference data for the ColourChecker come from the averaged measurement data available in [36]. The master calibration is performed once for a given calibration target in strictly controlled illumination conditions. It yields a reference CIE XYZ values for each marker, which are further used in a user calibration. Once the user model is known, it is used to derive the CIE XYZ coordinates of an arbitrary intensity input. In the last step, the final color representation is calculated by converting the CIE XYZ to sRGB color space coordinates [37].

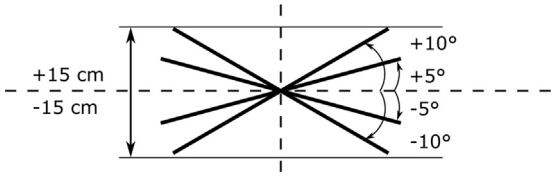

Fig. 6. Plane positioning during plane fitting tests.

Table 1
Exemplary results of plane fitting for measurements from different angles.

ID	Angle	Local fit 3σ	Global fit 1σ	Global fit 2σ	Global fit 3σ
a	-10°	0.078 mm	0.139 mm	0.282 mm	039 mm
b	-5°	0.084 mm	0.112 mm	0.239 mm	0.327 mm
c	5°	0.072 mm	0.103 mm	0.224 mm	0.309 mm
d	10°	0.089 mm	0.1547 mm	0.3007 mm	0.4 mm

Table 2
Exemplary results of plane fitting measurements from different distances.

ID	Distance	Local fit 3σ	Global fit 1σ	Global fit 2σ	Global fit 3σ
a	−5 cm	0.074 mm	0.0804 mm	0.164 mm	0.204 mm
b	0 cm	0.084 mm	0.078 mm	0.157 mm	0.2 mm
c	5 cm	0.087 mm	0.074 mm	0.161 mm	0.216 mm

4. RESULTS

4.1. System setup and hardware

Our main aim was to build a simple and cheap system to make 3D scans possible for regular customers in their houses. To achieve this goal we decided to simplify the calibration process and limit minimal required calibration target positions. Experimental system consists of an Optoma projector and a Point Grey camera with fixed focal length lens. The camera has to provide ability to set exposure settings, for example, its shutter, gain and white balance. In our opinion, nowadays (2016) the achieved accuracy of a point cloud is enough for home use.

4.2. Plane and sphere fitting

To measure accuracy and usability of the solution we decided to perform tests with planar and sphere references. As the plane reference we used the planar artifact used in the calibration. As mentioned in Section 3.1 the calibration artifact was made by gluing printed pattern onto 5 mm thick glass. We achieved planar target with flatness ≈ 1 μ. As the sphere reference, we used a validated reference provided by the Smarttech company. Radius of each sphere is equal to 18.750 ± 0.01 mm and distance between spheres is of 108.8 ± 0.01 mm. Procedures used during test were developed on the basis of ISO10360 [38] norm and VDI/VDE 2617-6 [39] recommendation.

4.2.1. Plane fitting

We performed plane fitting test in two parts. In the first part we placed the plane reference in the center of the measurement volume and performed measurements for different angles (Fig. 6). Distribution of errors are presented on Fig. 7.

For larger angles error distribution is cylindrical. We believe that this is a result of not exact representation of the spherical distortion in the distortion model (number of variables is constrained due to the lack of calibration data – only two artifact positions used). Quantitative results are shown in Table 1.

Second part includes measurements with the planar reference perpendicular to the camera optical axis in three positions: the centre of the measurement volume, and in positions closest and far-

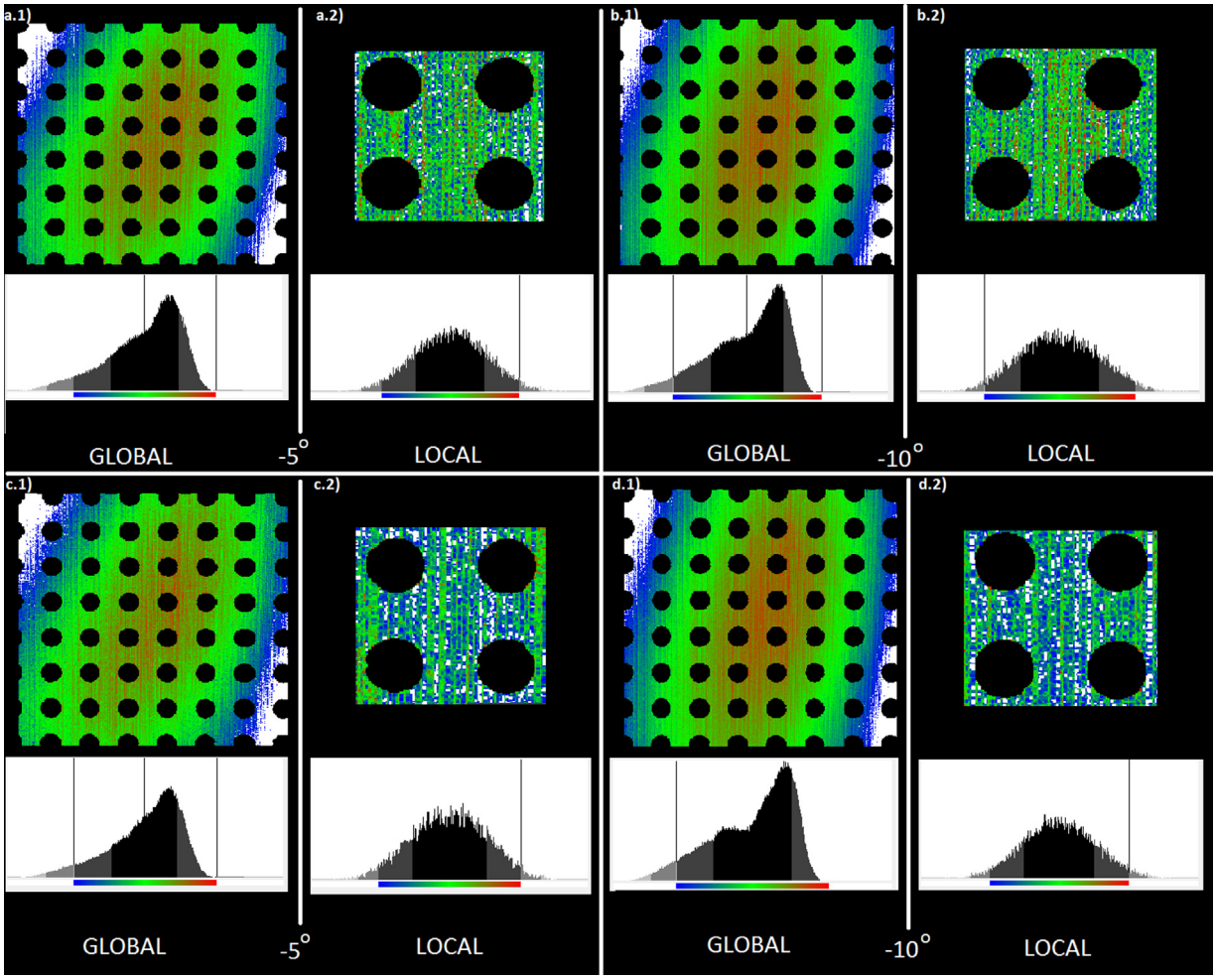

Fig. 7. Plane fitting for measurements from different angles. For each measurement plane the image with corresponding error distribution is presented. a.1–d.1 – results of the global plane fitting (for the whole plane), a.2–d.2 results of a local plane fitting (space between four markers). Quantitative values are presented in Table 1.

thest to the camera in the measurement volume. Error distributions are shown in Fig. 8, and values are shown in Table 2.

4.2.2. *Sphere fitting*

To assess the sphere fitting error we measured the SmartTech reference in 18 positions. For each position we calculated the best sphere approximation and estimated sphere fitting error. All error distributions were quasi-gaussian and fitting error values amounted to less than 11 μm. Example of sphere fitting error distribution is shown in Fig. 9, and all error values with corresponding distances from the center of the measurement volume are shown in Table 3.

4.2.3. *Distance*

Beside plane and sphere fitting, radius and distance calculation errors were tested. We used the reference with two spheres in this case. Measurements were performed for 9 reference positions. For every position the center and radius of each sphere reference was calculated. The results are presented in Table 4 It is worth mentioning that variance of error grows with the distance between sphere and the measurement volume center.

4.3. *Evaluation of colour reproduction*

To assess the accuracy of colour reproduction, an image of the X-Rite ColorChecker target was captured and reconstructed. The resulting CIE LAB coordinates were compared with reference values taken from the averaged measurements available in Ref. [36]. The average colour difference ΔE00 was calculated as a measure of accuracy for each colour patch. The result is shown in Fig. 10. For most of the patches the colour difference stays below ΔE00 = 5 which indicates perceptible deviation, but is considered sufficient. The solution focuses on improving color quality, regardless of users white balance and exposure setting and not on colourimetric accuracy.

4.4. *Real object measurement*

Beside tests mentioned above, we decided to perform a few measurements of real objects. We chose one object with complicated geometry and three simpler colour ones Fig. 11. For the gargoyle object we performed 12 measurements form different angles, aligned the resulting point clouds, merged them and made a mesh model (Fig. 12). For the remaining objects we performed measurements with colour correction. Resulting point clouds with texture are presented in Fig. 13.

4.5. *Comparison to existing systems*

In order to assess the quality of the proposed setup we decided to compare its performance with other 3d measurement optical systems. Different solutions require distinct calibration data, therefore it was not possible to directly compare results based on a common

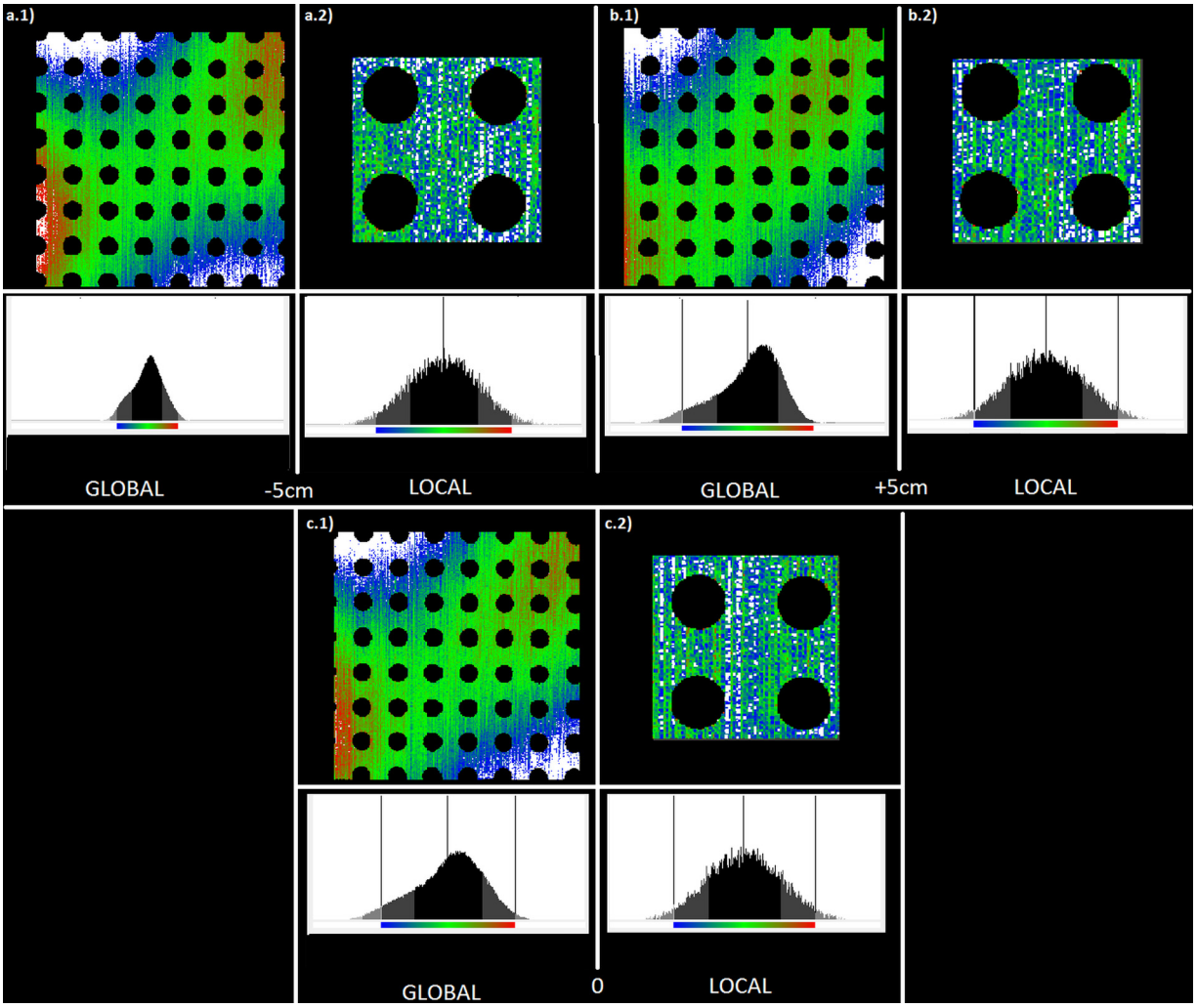

Fig. 8. Plane fitting for measurements from different distances. For each measurement plane the image with corresponding error distribution is presented. a.1–c.1 – results of the global plane fitting (for whole plane), a.2–c.2 results of a local plane fitting (space between four markers). Quantitative values are presented in Table 2.

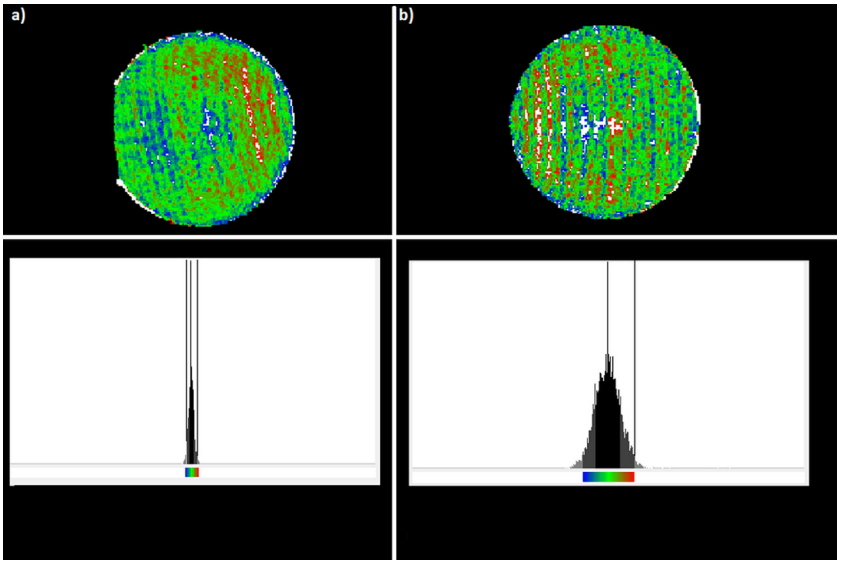

Fig. 9. Example of sphere fitting. Sphere image with the corresponding error distributions are presented. For each sphere calculation 3σ error ≤ 0.09 mm.

Table 3
Exemplary results of sphere fitting in different measurement volume locations.

ID	x-x_0 [mm]	y-y_0 [mm]	z-z_0 [mm]	Volume distance [mm]	Fit 3σ
1	8.13	-71.68	-14.32	73.55	0.081
2	4.47	36.92	-9.11	38.29	0.098
3	-51.67	-70.56	-29.34	92.25	0.081
4	-55.54	38.04	-23.74	71.38	0.096
5	114.04	-71.75	-27.39	137.49	0.0102
6	110.29	36.83	-21.99	118.34	0.0103
7	6.02	-72.78	4.12	73.14	0.085
8	2.09	35.79	9.71	37.15	0.099
9	-81.58	-72.5	9.59	109.56	0.086
10	-85.55	36.12	15.53	94.15	0.096
11	118.16	-73.38	0.33	139.09	0.01
12	114.32	35.16	5.56	119.73	0.097
13	24.06	-74.62	48.41	92.14	0.096
14	20.28	33.91	53.95	66.87	0.093
15	-72.56	-72.94	32.06	107.76	0.088
16	-76.26	35.73	37.33	92.12	0.095
17	122.54	-75.28	46.47	151.13	0.09
18	118.53	33.17	51.73	133.51	0.092

Table 4
Exemplary results of radius and two sphere distance calculation.

ID	x-x_0 [mm]	y-y_0 [mm]	z-z_0[mm]	Volume distance [mm]	Mean Dist	R	Rerr	Distance	distErr
1	8.13	-71.68	-14.32	73.55	55.92	18.726	0.024	108.789	0.011
2	4.47	36.92	-9.11	38.29	–	18.721	0.029	–	–
3	-51.67	-70.56	-29.34	92.25	81.81	18.644	0.106	108.814	0.014
4	-55.54	38.04	-23.74	71.38	–	18.639	0.111	–	–
5	114.04	-71.75	-27.39	137.49	127.91	18.844	0.094	108.783	0.017
6	110.29	36.83	-21.99	118.34	–	18.832	0.082	–	–
7	6.02	-72.78	4.12	73.14	55.14	18.725	0.025	108.787	0.013
8	2.09	35.79	9.71	37.15	–	18.718	0.032	–	–
9	-81.58	-72.5	9.59	109.56	101.86	18.63	0.12	108.857	0.057
10	-85.55	36.12	15.53	94.15	–	18.613	0.137	–	–
11	118.16	-73.38	0.33	139.09	129.41	18.86	0.11	108.739	0.061
12	114.32	35.16	5.56	119.73	–	18.839	0.089	–	–
13	24.06	-74.62	48.41	92.14	79.51	18.756	0.006	108.735	0.065
14	20.28	33.91	53.95	66.87	–	18.797	0.047	–	–
15	-72.56	-72.94	32.06	107.76	99.94	18.643	0.107	108.855	0.055
16	-76.26	35.73	37.33	92.12	–	18.631	0.119	–	–
17	122.54	-75.28	46.47	151.13	142.32	18.889	0.139	108.646	0.154
18	118.53	33.17	51.73	133.51	–	18.865	0.115	–	–

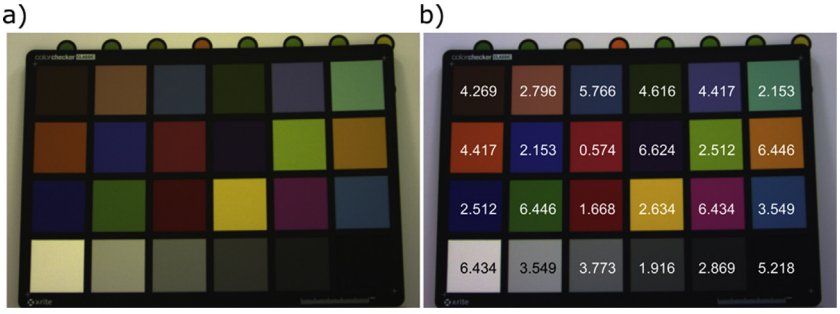

Fig. 10. Evaluation of colour reproduction accuracy: a) image of the ColourChecker target before correction; b) ColourChecker target after correction with embedded average ΔE00 of each patch.

Table 5
Comparison to existing systems.

Method	Input	Hardware	Absolute Accuracy	Measurement dimension	Relative Accuracy
Kinect 1.0 [41] Zhang calibration	10 images of planar pattern	IR camera, IR projector, RGB camera	~4 cm	5 m	0.8%
Camera and time-of-flight sensor [42]	5 images of planar pattern	Two RGB cameras, TOF sensor	~2 cm	~3 m	0.6%–1.8%
Structured light with sine fringe projection [40]	6 images of planar pattern +4 images with structured light projection	RGB camera, projector	~0.04 mm	1.2 m	0.036%
Proposed system	2 images of planar pattern with stuctured light projection	RGB camera, projector	0.4 mm	0.3 m	0.13%

Fig. 11. Objects chosen for test measurement (gargoyle, dancer,ship,thug.

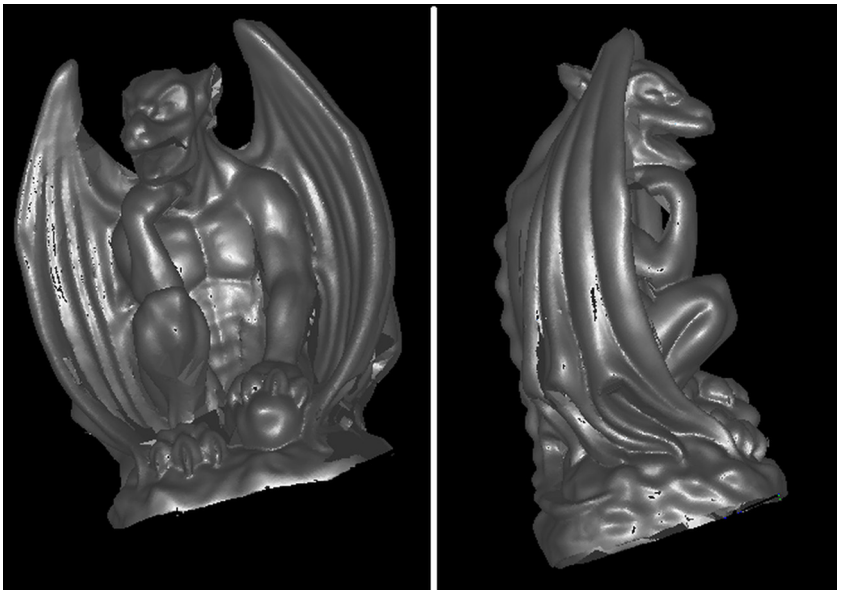

Fig. 12. Gargoyle mesh model exemplary views.

Fig. 13. Colour point clouds for chosen objects.

sample. Instead, an originally reported characteristics and relative accuracy was investigated, as presented in Table 5.

Our solution provides a compromise between high-accuracy, but more complicated approach, such as widely used fringe projection technique [40], and single frame based solutions, e.g. Kinect [41] and Time-of-Flight [42]. It offers very simple calibration procedure and relatively good accuracy, making it an interesting solution for industrial applications.

5. Conclusions

As a result of the conducted research a new procedure of calibration was developed and tested. Test results show, that with the use of the proposed method, the global measurement accuracy ≈ 0.4 mm and the local measurement accuracy ≈ 0.1 mm could be achieved. Colour calibration results are considered to be accurate enough for everyday and commercial use. Among many applications of SLS 3D measurement, the method introduced in this paper stands out by the fact of its simplicity and low cost of implementation. In spite of slightly lower accuracy, it allows the unqualified user to perform a complete 3D scan with integrated colour calibration. The presented method could be used to build cheap and reliable personal scanners for individual users and for educational purposes

Acknowledgements

This research was conducted for the SMARTTECH Company as a part of ACTPHAST (Access Center for Photonics Innovation Solutions and Technology Support) project “A low-cost 3D scanner with calibrated color measurement”. It was partially supported by statutory work of Warsaw University of Technology.

References

[1] R. Labayrade, D. Aubert, J.-P. Tarel, Real time obstacle detection in stereovision on non flat road geometry through “v-disparity” representation, Intell. Veh. Symp. 2 (2002) 646–651.
[2] M. Witkowski, R. Sitnik, M. Kujawiska, W. Rapp, M. Kowalski, B. Haex, S. Mooshake, 4d measurement system for automatic location of anatomical structures, Proc. SPIE 6191 (2006), 61910H–61910H–11.
[3] C. Liguori, A. Paolillo, A. Pietrosanto, An on-line stereo-vision system for dimensional measurements of rubber extrusions, Measurement 35 (2004) 221–231.
[4] J.J. Aguilar, M. Lope, F. Torres, A. Blesa, Development of a stereo vision system for non-contact railway concrete sleepers measurement based in holographic

optical elements. Measurement, J. Int. Meas. Confederation 38 (2) (2005) 154–165.
[5] J. Geng, Structured-light 3d surface imaging: a tutorial, Adv. Opt. Photonics 3 (2) (2011) 128–160.
[6] J. Salvi, S. Fernandez, T. Pribanic, X. Llado, A state of the art in structured light patterns for surface profilometry, Pattern Recog. (Vol 43, 2010).
[7] R. Sitnik, J. Woznicki, et al., Digital fringe projection system for large-volume 360-deg shape measurement, Opt. Eng. 41 (2) (2002) 443–449.
[8] J. Schanda, Colorimetry: understanding the CIE system, John Wiley & Sons, 2007.
[9] Z. Li, Accurate calibration method for a structured light system, Opt. Eng. 47 (5) (2008) 053604.
[10] F. Chen, G.M. Brown, M. Song, Overview of three-dimensional shape measurement using optical methods, Opt. Eng. 39 (January (1)) (2000).
[11] R. Sitnik, New method of structure light measurement system calibration based on adaptive and effective evaluation of 3d-phase distribution, Opt. Metrol. 5856 (2005) 109–117.
[12] P. Hariharan, B.F. Oreb, T. Eiju, Digital phase-shifting interferometry: a simple error-compensating phase calculation algorithm, Appl. Opt. 26 (5) (1987) 2504–2506.
[13] J.A. Quiroga, E. Bernabeu, Phase-unwrapping algorithm for noisy phase-map processing, Appl. Opt. 33 (29) (1994) 6725–6731.
[14] S. Zhang, S.-T. Yau, High-resolution, real-time 3d absolute coordinate measurement based on a phase-shifting method, Opt. Express 14 (7) (2006) 2644–2649.
[15] M. Axholt, Pinhole camera calibration in the presence of human noise, in: Doctoral thesis, LiU-Tryck, Linkoping, Sweden, 2011.
[16] X. Mei, S. Yang, J. Rong, X. Ying, S. Huang, H. Zha, Radial lens distortion correction using cascaded oneparameter division model, Image Processing (ICIP) IEEE International Conference (2015) 3615–3619.
[17] Y. Tang, Y. Li, J. Luo, Parametric distortion-adaptive neighborhood for omnidirectional camera, Appl. Opt. 54 (23) (2015) 6969–6978.
[18] O.D. Faugeras, Three-dimensional computer vision: A geometric viewpoint, MIT Press, 1993.
[19] Z. Zhang, A flexible new technique for camera calibration, IEEE Trans. Pattern Anal. Mach. Intell. 2000 (22) (2009) 1330–1334.
[20] J.J. More, The levenberg-marquardt algorithm: Implementation and theory, Numer. Anal. 630 (1978) 105–116.
[21] B.E. Bayer. Color imaging array. US patent 3971065, Issued 1976–07–20.
[22] C. Mauer, D. Wueller, Measuring the spectral response with a set of interference filters, Proc. SPIE 7250 (2009), 72500S–72500S–10.
[23] S. Lin , L. Zhang. Determining the radiometric response function from a single grayscale image, IEEE Computer Society Conference on Computer Vision and Pattern Recognition (CVPR'05) 2005 2.
[24] M.D. Grossberg, S.K. Nayar, Modeling the Space of Camera Response Functions, IEEE Trans. Pattern Anal. Mach. Intell. 26 (10) (2004) 1272–1282.
[25] G. Wyszecki, W.S. Stiles, Color Science. Concepts and Methods, Quantitative Data and Formulae, John Wiley & Sons, 2000, pp. 117–173.
[26] J.Y. Hardeberg, Acquisition and reproduction of color images: colorimetric and multispectral approaches, École Nationale Supérieure des Télécommunication, 2001, PhD thesis.
[27] H. Anwar, I. Din, K. Park, Projector calibration for 3d scanning using virtual target images, Int. J. Precis. Eng. Manuf. 13 (1) (2012) 125–131.
[28] J. Draréni, J. Roy, P. Sturm, Methods for geometrical video projector calibration Mach, Vision Appl. 23 (1) (2011) 79–89.
[29] J.S. Wheat, S. Choppin, A. Goyal, Development, assessment of a microsoft kinect based system for imaging the breast in three dimensions, Med. Eng. Phys. 36 (6) (2014) 732–738.
[30] D. Moreno, G. Taubin, 2012. Simple, accurate, and robust projector-camera calibration, 2nd International Conference on 3D Imaging, Modeling, Processing, Visualization and Transmission (3DIMPVT), October, 464–471.
[31] H. Saito, Y. Sato, K. Yamauchi, Calibration of a structured light system by observing planar object from unknown viewpoints, 19th International Conference on Pattern Recognition ICPR2008, Keio Univ.,Yokohama, Japan, 2008.
[32] J. Wilm, O.V. Olesen, R. Larsen, Accurate and simple calibration of dlp projector systems, Proc. SPIE 8979 (2014) 1–9.
[33] J. Weng, P. Cohen, M. Herniou, Camera calibration with distortion models and accuracy evaluation, IEEE Trans. Pattern Anal. Mach. Intell. 10 (1992) 965–980.
[34] R.I. Hartley, P. Sturm, Computer vision and image understanding, Triangulation 68 (2) (1997) 146–157.
[35] J.F. Blinn, A homogeneous formulation for lines in 3 space, ACM SIGGRAPH Comput. Graphics 11 (1977) 237–241, ACM.
[36] D. Pascale, RGB coordinates of the Macbeth ColorChecker, 2006. http://www.babelcolor.com/index_htm_files/RGB%20Coordinates%20of%20the%20Macbeth%20ColorChecker.pdf. (Accessed: 25 March 2016).
[37] IEC 61966–2-1:1999. Multimedia systems and equipment. Colour measurement and management. Colour management. Default RGB colour space: sRGB.
[38] ISO 10360–2:2009 geometrical product specifications (gps) – acceptance and reverification tests for coordinate measuring machines (cmm) – part 2: Cmms used for measuring linear dimensions, 2009.
[39] Vdi/vde 2617–6, accuracy of cmms – guideline for the application of iso 10360 to cmms with optical distance sensors, 1997.
[40] R. Sitnik, M. Kujawinska, J. Woznicki, Digital fringe projection system for large-volume 360-deg shape measurement, Opt. Eng. 41 (2) (2002) 443–449.
[41] K. Khoshelham, S.O. Elberink, Accuracy and resolution of kinect depth data for indoor mapping applications, Sensors 12 (2) (2012) 1437.
[42] J. Zhu, L. Wang, R. Yang, J. Davis, Fusion of time-of-flight depth and stereo for high accuracy depth maps, in: Computer Vision and Pattern Recognition, CVPR 2008, June, 2008, pp. 1–8.